

Legendre-Tau Spectral Elements for Incompressible Navier-Stokes Flow

Kelly Black*

Abstract

A spectral multi-domain method is introduced and examined. After dividing the computational domain into non-overlapping subdomains a Legendre-Tau approximation is constructed within each subdomain. Unlike the standard Legendre-Tau approximation a variational approximation is constructed and the result is that only simple continuity is required at the interfaces between the subdomains. The method is introduced for a simple 1D Helmholtz equation and two examples are given: a 1D Burger's Equation with a small viscosity and Navier-Stokes incompressible flow over a backstep.

Key words: spectral elements, Helmholtz equation, Burger's equation, Navier-Stokes equation.

AMS subject classifications: 65N30, 65N35, 76D05.

1 Introduction

A spectral multi-domain approximation using a Lanczos-Tau approximation [4, p. 79] is examined and is implemented by enforcing a variational approximation. The method is constructed so as to construct a local spectral basis within each subdomain [3]. The method is first introduced for a simple Helmholtz equation, a 1D Burger's equation with a small viscosity, and finally the Navier-Stokes incompressible flow over a backstep is examined.

Another technique which yields an approximation in the Fourier domain has been proposed by Israeli, et al in [8], however the approach proposed here has more in common with the collocation method proposed by Patera [11]. A collocation method using the same test functions for the

*Department of Mathematics, University of New Hampshire, black@vidalia.unh.edu

ICOSAHOM'95: Proceedings of the Third International Conference on Spectral and High Order Methods. ©1996 Houston Journal of Mathematics, University of Houston.

variational form that is examined here has been proposed in [2]. Because a variational approach is employed the method has the advantage that the interface can be easily calculated by requiring only C^0 continuity.

Unlike other variational approaches an approximation is found in the Spectral domain. This approach easily takes advantage of the accuracy of the spectral multi-domain methods as well as an advantage in the robustness of the Galerkin schemes. The numerical schemes generated from such an approach can easily accommodate complicated boundary conditions that depend on the spectrum. One disadvantage is that any nonlinear terms are more expensive to compute when compared to the collocation approach. Because this approach is designed for use with multiple computational subdomains the size of the approximating space on each subdomain is kept small, and the expense of calculating the nonlinear terms can be kept low.

Because the scheme is essentially a Legendre-Tau method, the system of equations is constructed in the same manner as is done with Galerkin methods. Since the approximating functions do not necessarily satisfy the boundary conditions the boundaries are directly enforced. This is done either by enforcing the boundaries at specific grid points or by a minimization of the difference between the true boundaries and the approximation.

2 Multi-domain tau method

To take advantage of the high accuracy and relatively coarse discretizations offered by spectral methods and avoid restrictions placed on the computational domain, the domain is subdivided into non-overlapping subdomains. On each subdomain an approximation is found that is a linear combination of the Legendre polynomials up to a given degree. To present the method without the burden of too many technical details, first a simple 1D Helmholtz equation is examined,

$$(1) \quad \begin{aligned} u_{xx} + \lambda u &= f, & x \in (0, 1), \\ u(0) &= u(1) = 0. \end{aligned}$$

The approximation is constructed by integrating against a sequence of test functions and building a system of algebraic equations. In the standard implementation of the Tau method the test functions are chosen to be the same as the trial functions. In such a case both the test functions and the trial functions are found from the sequence of Legendre polynomials. Since a multi-domain approximation is sought the test functions, $\tilde{\psi}_j(x)$, are defined in a different way,

$$(2) \quad \begin{aligned} \tilde{\psi}_j(x) &= (1-x^2)L_j(x), & 0 \leq j < N-1, \\ \tilde{\psi}_{N-1}(x) &= \frac{1+x}{2}, \\ \tilde{\psi}_N(x) &= \frac{1-x}{2}. \end{aligned}$$

As defined the test functions are zero on the endpoints for $j = 0 \dots N-2$. For $j = N-1$ and $j = N$ the test functions are linear polynomials, and the span of all of the test functions is \mathbb{P}_N .

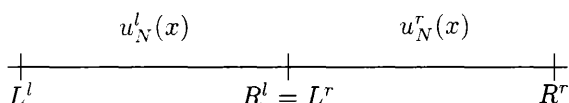


Figure 1: A Multi-Domain Example in 1-D for subdomains l and r .

The computational domain is to be divided into M non-overlapping subdomains. For a given subdomain, r , the approximation is written as $u_N^r(x) \in \mathbb{P}_N$ and the left and right endpoints are L^r and R^r , respectively (see Figure 1). On each subdomain the domain is mapped to the unit square $[-1,1]$ using a simple linear transformation:

$$(3) \quad \bar{x}^r = 2\frac{x-L^r}{R^r-L^r} - 1, \quad x \in [L^r, R^r].$$

The approximation on subdomain r is written as a linear combination of the Legendre polynomials and has support only on subdomain r :

$$(4) \quad u_N^r(x) = \begin{cases} \sum_{i=0}^N \alpha_j^r L_i(\bar{x}^r), & x \in [L^r, R^r] \\ 0 & \text{otherwise.} \end{cases}$$

In this example x is in the computational domain defined in equation (1) and \bar{x}^r is found from equation (3). For $0 \leq j \leq N$, the test functions for subdomain r are define,

$$(5) \quad \psi_j^r(x) = \begin{cases} \tilde{\psi}_j(\bar{x}^r) & x \in [L^r, R^r] \\ 0 & \text{otherwise.} \end{cases}$$

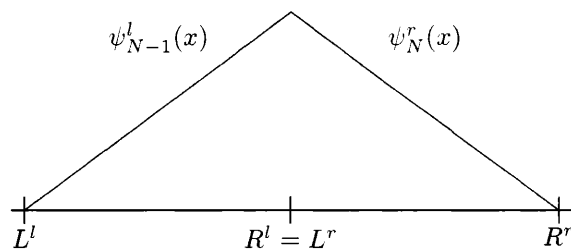


Figure 2: Trial functions $\psi_{N-1}^l(x)$ and $\psi_N^r(x)$ combine on adjacent subdomains to assemble an “hat” function.

With these definitions the variational approximation can be examined. Except for the linear functions, the test functions are zero on the subdomain boundaries, and each test function has support on only one subdomain. When integrating against the approximation the only integral that need be found is that part within the individual subdomain. The linear test functions, however, do not have zero boundaries on each subdomain. If the linear functions on adjacent subdomains are examined the result is a simple hat function (see Figure 2). This composite test function is used to insure that the flux is balanced across the subdomain interface.

By splitting the trial functions into the polynomials that are zero at the boundaries and those that are not, the method is a p -version finite element method. Unlike more conventional p -version schemes, by constructing the approximation as a linear combination of the Legendre polynomials it becomes quite easy to increase the order of the approximation within each subdomain (p -refinement). Moreover, the resulting matrices share a similar structure to those found in the conventional single subdomain Legendre-Tau method[4]. For example, within each subdomain the entries for the stiffness matrix corresponding to trial functions which are zero at the boundaries represent a sparse upper-triangular matrix.

Once the approximation and the test functions are defined on the two subdomains the variational approximation of equation (1) is constructed. For $j = 0, \dots, N-2$ the following equations are enforced on each subdomain:

$$(6) \quad \int_{L^r}^{R^r} - \left(\frac{d}{dx} u_N^r(x) \right) \left(\frac{d}{dx} \psi_j^r(x) \right) + \lambda u_N^r(x) \psi_j^r(x) dx = \int_{L^r}^{R^r} f_N^r(x) \psi_j^r(x) dx.$$

Assuming that subdomain l is the subdomain to the left and adjacent to subdomain r , the equations for the linear test functions are constructed by integrating against the

hat function:

$$\begin{aligned}
 & \int_{L^l}^{R^l} - \left(\frac{d}{dx} u_N^l(x) \right) \left(\frac{d}{dx} \psi_{N-1}^l(x) \right) + \lambda u_N^l(x) \psi_{N-1}^l(x) dx \\
 & + \int_{L^r}^{R^r} - \left(\frac{d}{dx} u_N^r(x) \right) \left(\frac{d}{dx} \psi_N^r(x) \right) + \lambda u_N^r(x) \psi_N^r(x) dx \\
 (7) \quad & = \int_{L^l}^{R^l} f_N^l(x) \psi_{N-1}^l(x) dx + \int_{L^r}^{R^r} f_N^r(x) \psi_N^r(x) dx.
 \end{aligned}$$

The boundary conditions are enforced as they are done in the standard Tau techniques. Assuming that subdomain 0 is the far left subdomain and M is the subdomain on the far right, the boundaries are directly enforced in a pointwise manner,

$$\begin{aligned}
 (8) \quad u_N^0(0) &= \sum_{i=0}^N \alpha_i^0 (-1)^i = 0, \\
 u_N^M(1) &= \sum_{i=0}^N \alpha_i^M = 0.
 \end{aligned}$$

The subdomain interfaces are enforced by simply requiring C^0 continuity:

$$\begin{aligned}
 (9) \quad u_N^l(R^l) &= u_N^r(L^r), \\
 \sum_{i=0}^N \alpha_i^l &= \sum_{i=0}^N \alpha_i^r (-1)^i.
 \end{aligned}$$

The solution to the system of equations in equations (6) through (9) is the approximation to equation (1).

2.1 The stiffness matrix

Equations (6) through (9) are used to construct an approximation to equation (1). By substituting $u_N^r(x)$ from equation (4) the stiffness and the mass matrices can be constructed. Here we will concentrate on the second derivative operator and find the entries for the stiffness matrix. The entries for the stiffness matrix are derived and the mass matrix can be found in a similar process.

The stiffness matrix is found by examining the variational form for the second derivative. After a substitution to allow for integration across $[-1, 1]$ the variational form of the second derivative in equation (6) is derived for $j = 0 \dots N - 2$:

$$\begin{aligned}
 & \int_{L^r}^{R^r} - \left(\frac{d}{dx} u_N^r(x) \right) \left(\frac{d}{dx} \psi_j^r(x) \right) dx \\
 & = \frac{-2}{R^r - L^r} \\
 & \int_{-1}^1 \left(\frac{d}{d\bar{x}^r} u_N^r \left(\frac{R^r - L^r}{2} (\bar{x}^r + 1) - L^r \right) \right) \\
 & \quad \left(\frac{d}{d\bar{x}^r} \tilde{\psi}_j(\bar{x}^r) \right) d\bar{x}^r.
 \end{aligned}$$

First, the sum of Legendre polynomials is substituted for the approximation $u_N^r(x)$. For $j = 0 \dots N - 2$ the result is

$$\begin{aligned}
 (10) \quad & \int_{L^r}^{R^r} - \left(\frac{d}{dx} u_N^r(x) \right) \left(\frac{d}{dx} \psi_j^r(x) \right) dx \\
 & = \sum_{i=0}^N \alpha_i^r \left(\frac{-2}{R^r - L^r} \right) \\
 & \quad \int_{-1}^1 L_i'(\bar{x}^r) \frac{d}{d\bar{x}^r} \left((1 - (\bar{x}^r)^2) L_j(\bar{x}^r) \right) d\bar{x}^r.
 \end{aligned}$$

The system of equations can be constructed through the use of a stiffness matrix, \mathcal{S}_N , by setting

$$\begin{aligned}
 (\mathcal{S}_N)_{ji} &= \frac{-2}{R^r - L^r} \int_{-1}^1 L_i'(x) \frac{d}{dx} \left((1 - x^2) L_j(x) \right) dx \\
 (11) \quad & = \frac{2}{R^r - L^r} \left(4e_{ji} + \frac{2j(1-j)}{2j+1} \delta_{ji} \right),
 \end{aligned}$$

for $0 \leq j < N - 1$, and $0 \leq i \leq N$ e_{ji} is given by

$$(12) \quad e_{ji} = \begin{cases} 1 & i+j \text{ even, } i \geq j+2 \\ 0 & \text{otherwise.} \end{cases}$$

This yields a sparse upper-triangular matrix and is similar to the result for the standard single domain tau method [4].

The equations for the interface are found by integrating against the hat function over the two subdomains as given in equation (7),

$$\begin{aligned}
 (13) \quad & \int_{L^l}^{R^l} - \left(\frac{d}{dx} u_N^l(x) \right) \left(\frac{d}{dx} \psi_{N-1}^l(x) \right) dx + \\
 & \int_{L^r}^{R^r} - \left(\frac{d}{dx} u_N^r(x) \right) \left(\frac{d}{dx} \psi_N^r(x) \right) dx \\
 & = \sum_{i=0}^N \alpha_i^l \left(-\frac{2}{R^l - L^l} \right) \int_{-1}^1 L_i'(\bar{x}^l) \frac{d}{d\bar{x}^l} \left(\frac{1 + \bar{x}^l}{2} \right) d\bar{x}^l + \\
 & \quad \sum_{i=0}^N \alpha_i^r \left(-\frac{2}{R^r - L^r} \right) \int_{-1}^1 L_i'(\bar{x}^r) \frac{d}{d\bar{x}^r} \left(\frac{1 - \bar{x}^r}{2} \right) d\bar{x}^r \\
 & = - \sum_{\substack{i=1 \\ i \text{ odd}}}^N \alpha_i^l \left(\frac{2}{R^l - L^l} \right) + \sum_{\substack{i=1 \\ i \text{ odd}}}^N \alpha_i^r \left(\frac{2}{R^r - L^r} \right)
 \end{aligned}$$

The entries for the stiffness matrix are found by enforcing the variational form of the second derivative as well as the boundaries. The mass matrix, \mathcal{M}_N , can be constructed using the same approach.

3 Burger's equation with a small viscosity

An example of the discretization for Burger's equation with a small viscosity is examined,

$$\begin{aligned} u_t + uu_x &= \nu u_{xx}, \quad x \in (-1, 1), \quad t > 0, \\ u(\pm 1, t) &= 0, \quad t > 0, \\ u(x, 0) &= -\sin(\pi x). \end{aligned}$$

This equation develops a steep gradient around $x = 0$ and has been examined in Basdevant, et al [1]. The temporal discretizations employed here closely parallel those found in [1].

The previously described spatial discretization is employed in the approximation to equation (14). The temporal discretization is constructed from a finite difference approximation and employs an Adams-Bashforth/Crank-Nicholson Scheme (ABCN) [1]. The approximation at the n^{th} time step is denoted u_N^n . The convective term is approximated using the explicit Adams-Bashforth discretization and the diffusive term is approximated using the implicit Crank-Nicholson discretization,

$$(14) \quad \begin{aligned} \hat{u}_N^n &= u_N^n (u_N^n)_x, \\ \frac{u_N^{n+1} - u_N^n}{\Delta t} &= \frac{1}{2}(-3\hat{u}_N^n + \hat{u}_N^{n-1}) \\ &\quad + \frac{\Delta t \nu}{2} ((u_N^{n+1})_{xx} + (u_N^n)_{xx}), \end{aligned}$$

and the resulting matrix equations are given by

$$(15) \quad \begin{aligned} \hat{u}_N^n &= u_N^n (u_N^n)_x, \\ \mathcal{C} u_N^n &= \mathcal{M} \frac{\Delta t}{2} (-3\hat{u}_N^n + \hat{u}_N^{n-1}) + \mathcal{D} u_N^n, \\ \mathcal{C} &= \mathcal{M} - \frac{\Delta t \nu}{2} \mathcal{S}, \\ \mathcal{D} &= \mathcal{M} + \frac{\Delta t \nu}{2} \mathcal{S}. \end{aligned}$$

The nonlinear terms can be calculated as a convolution sum [4, p. 82] or using collocation on the abscissa from the Gauss-Lobatto quadrature as was done here [4, p. 83].

A comparison between three different methods is examined. The first is a single domain Chebychev-Tau scheme [4, p. 80], a Chebychev-Galerkin-Collocation scheme [11], and a multi-domain Legendre-Tau scheme. (A comparison between a finite difference approximation and the spectral techniques can be found in [1].) For the two spectral element approximations four equally spaced subdomains are implemented. In the examples the values $\nu = \frac{1}{100\pi}$, $\Delta t = \frac{1}{200\pi}$ are employed.

The true solution that is used for reference is approximated from the convolution product given in Cole's transformation [5]. An approximation of the true solution was calculated using Gauss-Hermite integration with 9 digits of accuracy [6, 12]. (For $\nu = \frac{1}{100\pi}$ the gradient achieves its maximum near $t = 0.5$ [1].)

The L^2 errors for these values are given in Figures 3 through 5. For this test case the L^2 errors are presented for the times $t = 1/\pi$, $t = 2/\pi$, and $t = 3/\pi$ [1]. For each of the three trials the error reported is not the percentage error. In the test case a steep gradient occurs around $x = 0$ and once this gradient is resolved the two multi-domain methods offer a more accurate approximation.

Figures 3 through 5 demonstrate that the multi-domain techniques can yield a more accurate approximation when compared to a single domain approximation. Because the steep gradient occurs around a subdomain interface the two multi-domain techniques are better able to resolve the gradient. The approximations at the times $2/\pi$ and $3/\pi$ demonstrates the robustness of the Tau approximations. When the gradient is not adequately resolved the collocation scheme actually diverges while both Tau methods maintain their stability. The multi-domain Tau method maintains the advantages of both the Tau method and the multi-domain method.

4 Navier-Stokes incompressible flow

The incompressible Navier-Stokes flow equation.

$$(16) \quad \begin{aligned} u_t + (u \cdot \nabla)u + \nabla p &= \frac{1}{\text{Re}} \nabla^2 u, \\ \text{subject to } \nabla \cdot u &= 0, \end{aligned}$$

with no slip boundaries are examined [7]. The geometries examined are for flow within a driven cavity as well as flow over a backstep. The spatial discretization employed is the same as examined in section 2. The temporal discretization is based on the the splitting method [10] and the methods proposed by Karniadakis, et al [9]. The splitting method is a convenient scheme to separate the actions of the two spatial operators acting on the velocity,

$$(17) \quad \begin{aligned} \mathcal{N}(u) &= \frac{1}{2} ((u \cdot \nabla)u + \nabla \cdot (uu)), \\ \mathcal{L}(u) &= \frac{1}{\text{Re}} \nabla^2 u. \end{aligned}$$

(The implementation employs the skew-symmetric form of the nonlinear operator).

Approximation to Burger's Equation - L² Errors

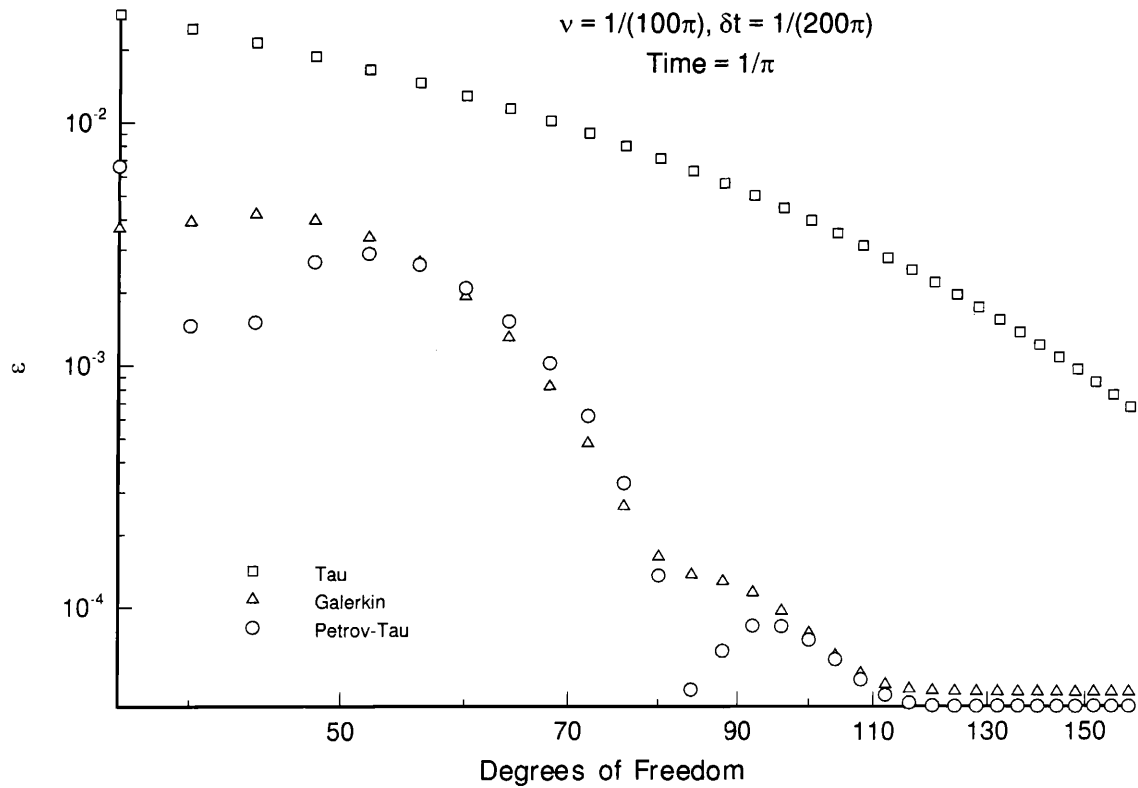


Figure 3: The L² errors for the approximation to Burger's Equation with a small viscosity at the time $t = \frac{1}{\pi}$.

Following the method proposed by Karniadakis, et al [9], the pressure is not calculated, rather the time averaged pressure is approximated. The three relevant spatial operators can then be isolated in three separate steps,

$$\begin{aligned}
 (18) \quad \tilde{u}_N - u_N^n &= - \int_{t_n}^{t_{n+1}} \mathcal{N}(u_N) dt, \\
 -\tilde{u}_N + \hat{u}_N &= -\nabla \bar{p}, \quad \text{subject to } \nabla \cdot \hat{u}_N = 0, \\
 u_N^{n+1} - \hat{u}_N &= \int_{t_n}^{t_{n+1}} \mathcal{L}(u_N) dt.
 \end{aligned}$$

In the first time step the nonlinear term is integrated through the use of an explicit method such as those from the Adams-Bashforth family of schemes while the third step employs an implicit step such as those found in the Adams-Moulton family of schemes. Because an explicit step is taken there is a restriction on the time step. However, the more stringent restriction on the time step comes

from the Stokes operator. This is mitigated through the use of the implicit step in the final equation.

For the 2D equations the both the approximating and trial functions are taken as tensor products of those found in the 1D case. Within each subdomain an approximation is constructed which is a linear combination of the Legendre polynomials, for (x, y) in subdomain r ,

$$(19) \quad u_N^r(x, y) = \sum_{j=0}^N \sum_{i=0}^N \alpha_{ij}^r L_i(\bar{x}^r) L_j(\bar{y}^r).$$

The test functions are also found as a simple tensor product, $\psi_j^r(\bar{x}^r) \psi_i^r(\bar{y}^r)$.

Continuity across the subdomain interfaces are enforced by minimizing the difference between the approximations on adjacent subdomains. For example, if subdomain r is to the right of subdomain l then on subdomain r the boundary $\bar{x}^r = -1$ is adjacent to the boundary on subdomain l

Approximation to Burger's Equation - L² Errors

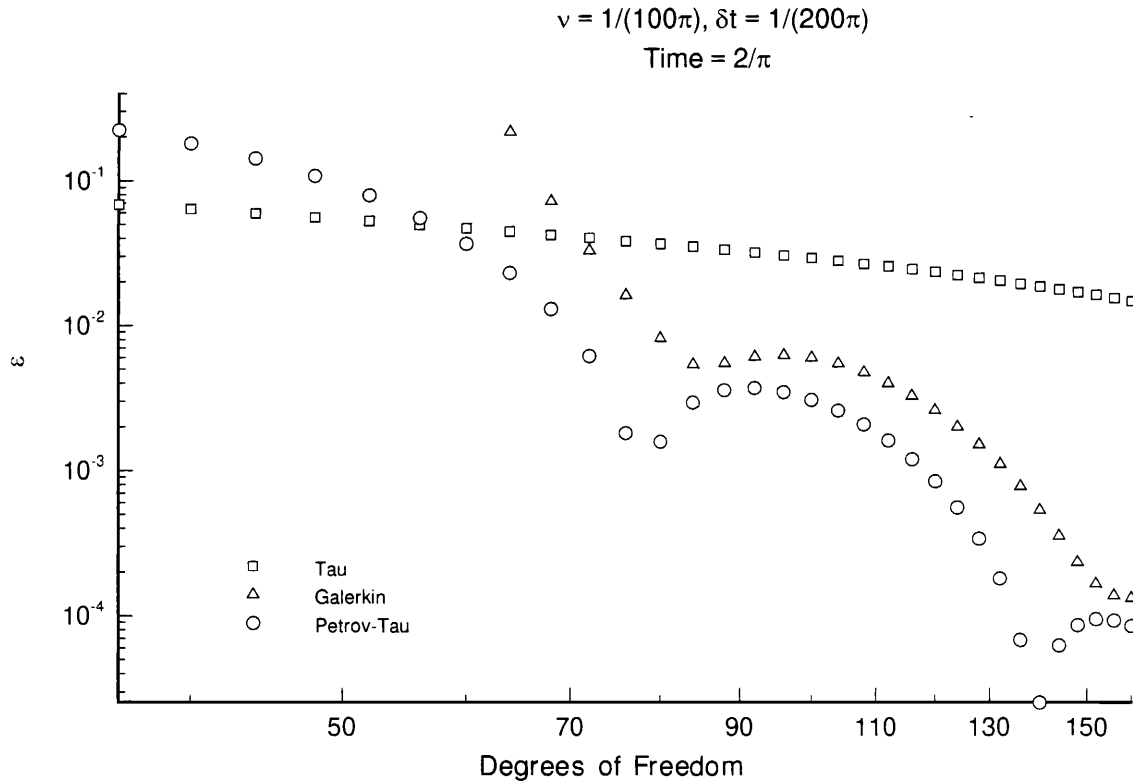


Figure 4: The L² errors for the approximation to Burger's Equation with a small viscosity at the time $t = \frac{2}{\pi}$.

when $\bar{x}^l = 1$. The continuity across this interface is enforced by requiring that the difference between the two approximations be orthogonal to the space of polynomials of degree $N - 2$,

$$(20) \quad \int_{-1}^1 (u_N^l(1, y) - u_N^r(-1, y)) L_j(y) dy = 0, \quad j = 0 \dots N - 2.$$

Continuity is ensured with the final requirement that the subdomains be continuous at the corners which is directly enforced as it is done with collocation type methods,

$$(21) \quad \begin{aligned} u_N^l(1, 1) &= u_N^r(-1, 1), \\ \sum_{i=0}^N \sum_{j=0}^N \alpha_{ij}^l &= \sum_{i=0}^N \sum_{j=0}^N (-1)^i \alpha_{ij}^r, \end{aligned}$$

and,

$$(22) \quad \begin{aligned} u_N^l(1, -1) &= u_N^r(-1, -1), \\ \sum_{i=0}^N \sum_{j=0}^N (-1)^j \alpha_{ij}^l &= \sum_{i=0}^N \sum_{j=0}^N (-1)^j (-1)^i \alpha_{ij}^r. \end{aligned}$$

4.1 Flow over a Backstep

In the second trial, the Navier-Stokes incompressible flow over a backstep, the domain is divided into 30 subdomains (see Figure 7). On each subdomain the approximation utilizes a polynomial of degree 6 in both the x and the y -directions. The initial condition is zero velocity with a time step of $\Delta t = 10^{-3}$. The height of the backstep is 1 and the maximum velocity at the inlet is 1. The implicit step that is taken in equation (18) is inverted through the use of the GMRES method [13, 14].

Approximation to Burger's Equation - L^2 Errors

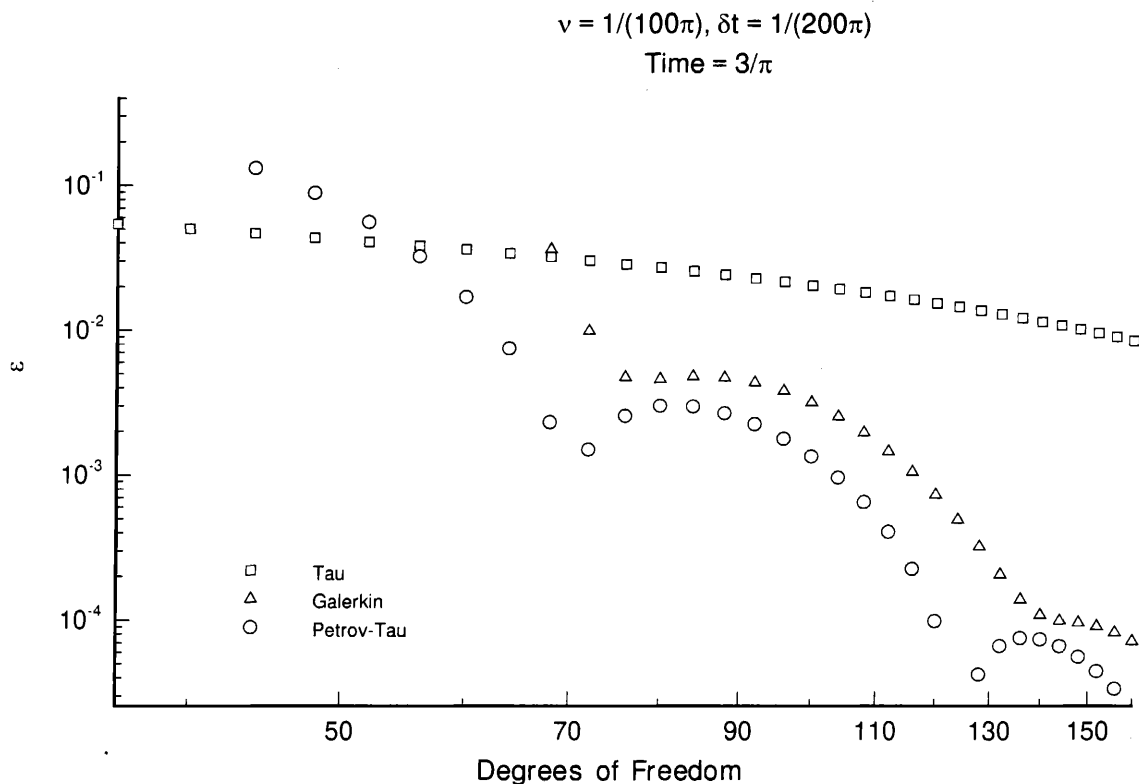


Figure 5: The L^2 errors for the approximation to Burger's Equation with a small viscosity at the time $t = \frac{3}{\pi}$.

In this example two different Reynolds numbers are examined, $Re = \frac{1}{200}$ and $Re = \frac{1}{400}$ and the velocity fields are shown in Figure 8. For the situation for $Re = \frac{1}{200}$ the initial velocity was taken to be zero and the velocity field shown was found after 6000 time steps. For the situation for $Re = \frac{1}{400}$ the initial condition employed was the velocity field obtained in the previous situation. The velocity field shown was found after 2300 time steps.

Figures 8 and 9 show the velocity fields for both trials. The first figure, Figure 8, demonstrates the velocity field for the area around the inlet and the backstep. The second figure, Figure 9, is a more detailed view of the area directly behind the backstep itself and shows the area of recirculation.

References

- [1] Basdevant, C., M. Deville, P. Haldenwang, J.M. Lacroix, J. Ouazzani, R. Peyret, P. Orlandi and A.T. Patera, *Spectral and Finite Difference Solutions of the Burger's Equation*, Computers and Fluids, 14 (1986), pp. 23-41.
- [2] Black, K., *A Petrov-Galerkin Spectral Element Technique for Heterogeneous Porous Media Flow*, International Journal of Computers in Mathematics and Applications, 29 (1995), pp. 49-65.
- [3] Black, K., *Legendre-Tau Spectral Elements for Incompressible Navier-Stokes Flow*, 1995. Accepted for the proceedings of the ICOSAHOM 95 Conference.

True Solution to Burger's Equation With a Viscosity

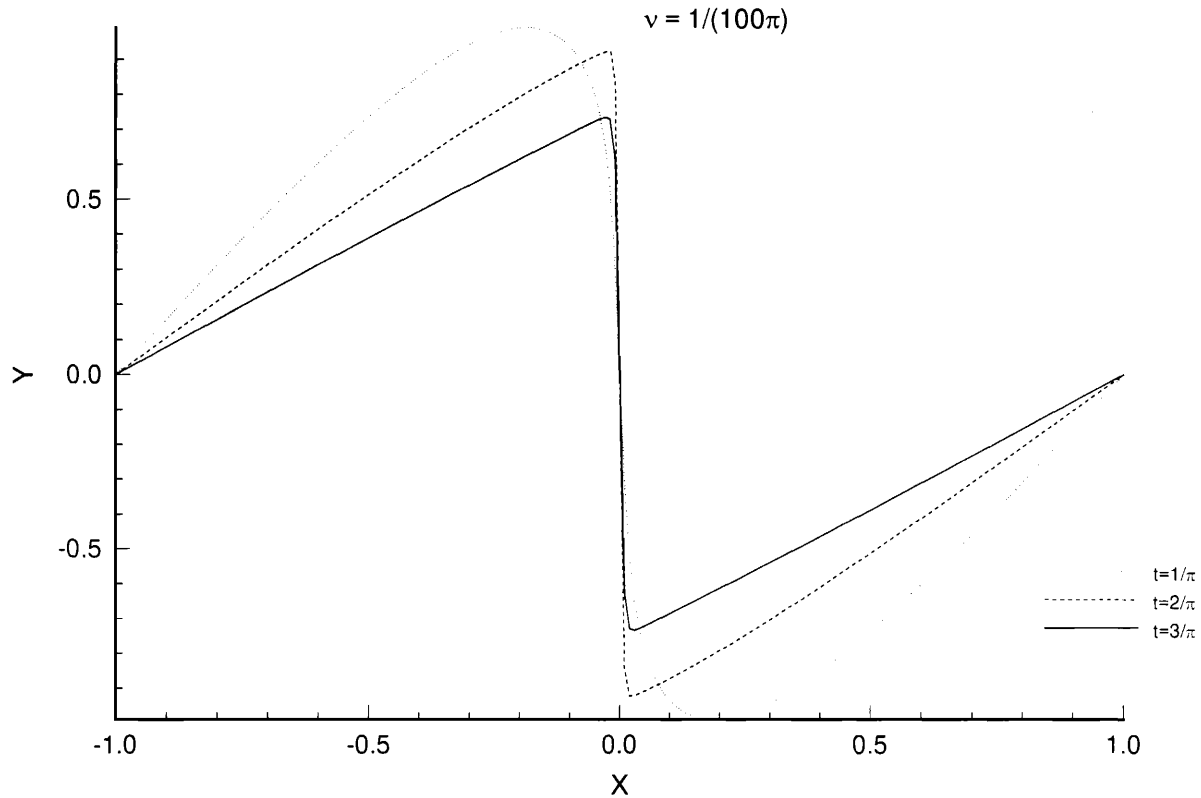


Figure 6: The true solution to Burger's Equation at $t = \frac{1}{\pi}$, $t = \frac{2}{\pi}$, and $t = \frac{3}{\pi}$.

- [4] Canuto, C., Hussaini, M.Y., Quarteroni, A., and Zang, T.A., *Spectral Methods in Fluid Dynamics*, Springer-Verlag, New York, 1988.
- [5] Cole, Julian D., *On a Quasi-Linear Parabolic Equation Occuring in Aerodynamics*, Quarterly of Applied Mathematics, IX (1951), pp. 225–236.
- [6] Davis, Philip J. and Rabinowitz, Philip, *Methods of Numerical Integration*, Academic Press, inc. (Harcourt Brace Jovanovich), New York, second ed., 1984.
- [7] Gresho, Philip M., and Robert L. Sani, *On Pressure Boundary Conditions for the Incompressible Navier-Stokes Equations*, International Journal for Numerical Methods in Fluids, 7 (1987), pp. 1111–1145.
- [8] Israeli, M., L. Vozovoi and A. Averbach, *Spectral Multidomain Technique with Local Fourier Basis*, Journal of Scientific Computing, 8 (1993), pp. 135–149.
- [9] Karniadakis, G., M. Israeli, and S. Orszag, *High-Order Splitting Methods for the Incompressible Navier-Stokes Equations*, Journal of Computational Physics, 97 (1991), pp. 414–443.
- [10] Maday, Y., A. Patera, and E. Rønquist, *An Operator-Integration-Factor Splitting Method for Time-Dependant Problems: Application to Incompressible Flow*, Journal of Scientific Computing, 5 (1990), pp. 263–292.
- [11] Patera, Anthony T., *A Spectral Element Method for Fluid Dynamics: Laminar Flow in a Channel Expansion*, Journal of Computational Physics, 54 (1984), pp. 468–488.

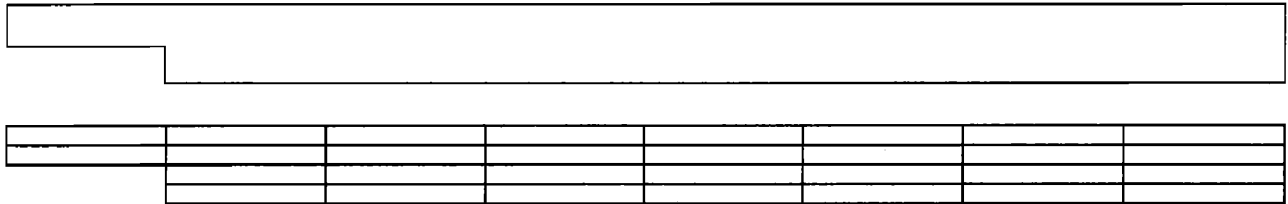


Figure 7: Graph of the geometry for the backstep. The backstep has height 1 and the maximum velocity at the inlet is 1. The domain is divided into 30 subdomains and a spectral approximation is constructed within each subdomain. Within each subdomain a Legendre polynomial approximation is employed with the degree of the polynomial 6 in the x -direction and 6 in the y -direction.

- [12] Press, William, S. Teukolsky, W. Vetterling, and B. Flannery, *Numerical Recipes in C*, Cambridge University Press, New York, second ed., 1992.
- [13] Saad, Youcef, and Martin Schultz, *GMRES: A Generalized Minimal Residual Algorithm for Solving Nonsymmetric Linear Systems*, *Siam Journal of Scientific and Statistical Computing*, 7 (1986), pp. 856–869.
- [14] Walker, Homer F., *Implementation of the GMRES Method Using Householder Transformations*, *Siam Journal of Scientific and Statistical Computing*, 9 (1988), pp. 152–163.

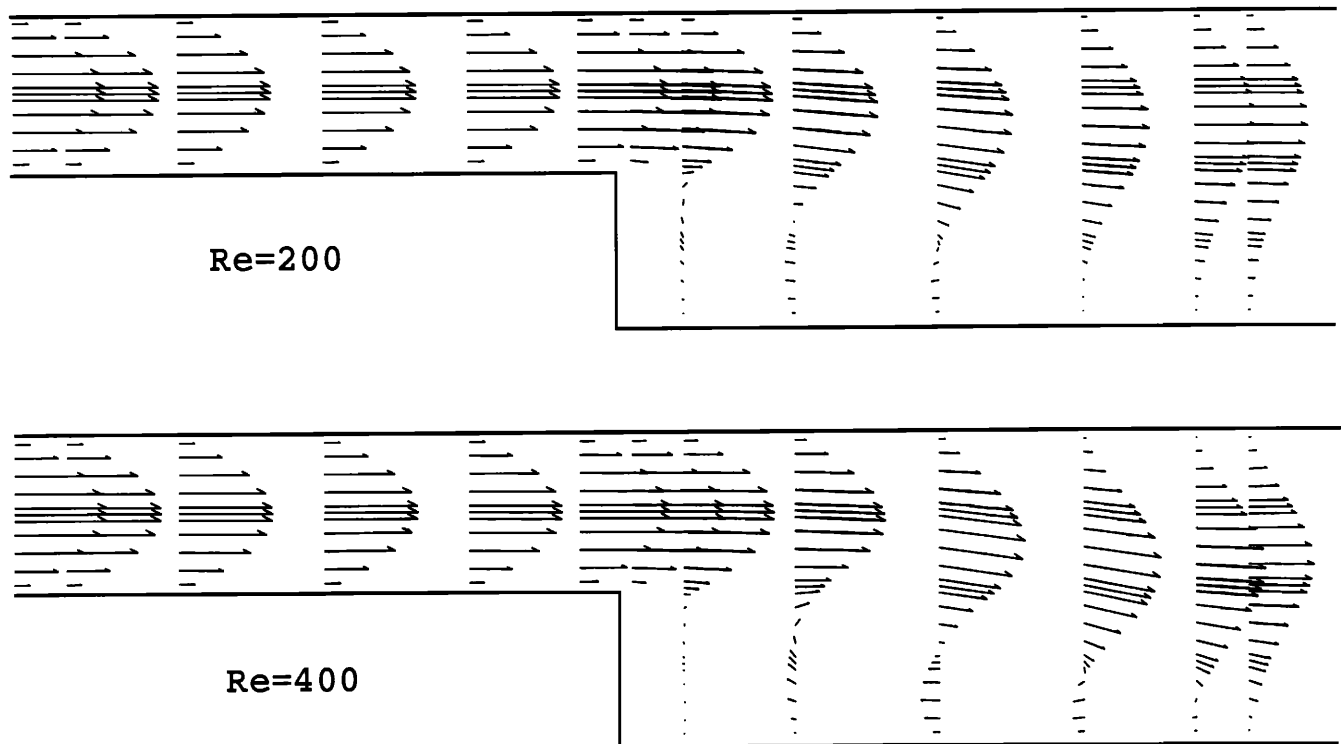


Figure 8: Vector plot for the inlets for two simulations. The top simulation is from the test case $Re=200$ and the bottom simulation is from the test case $Re=400$.

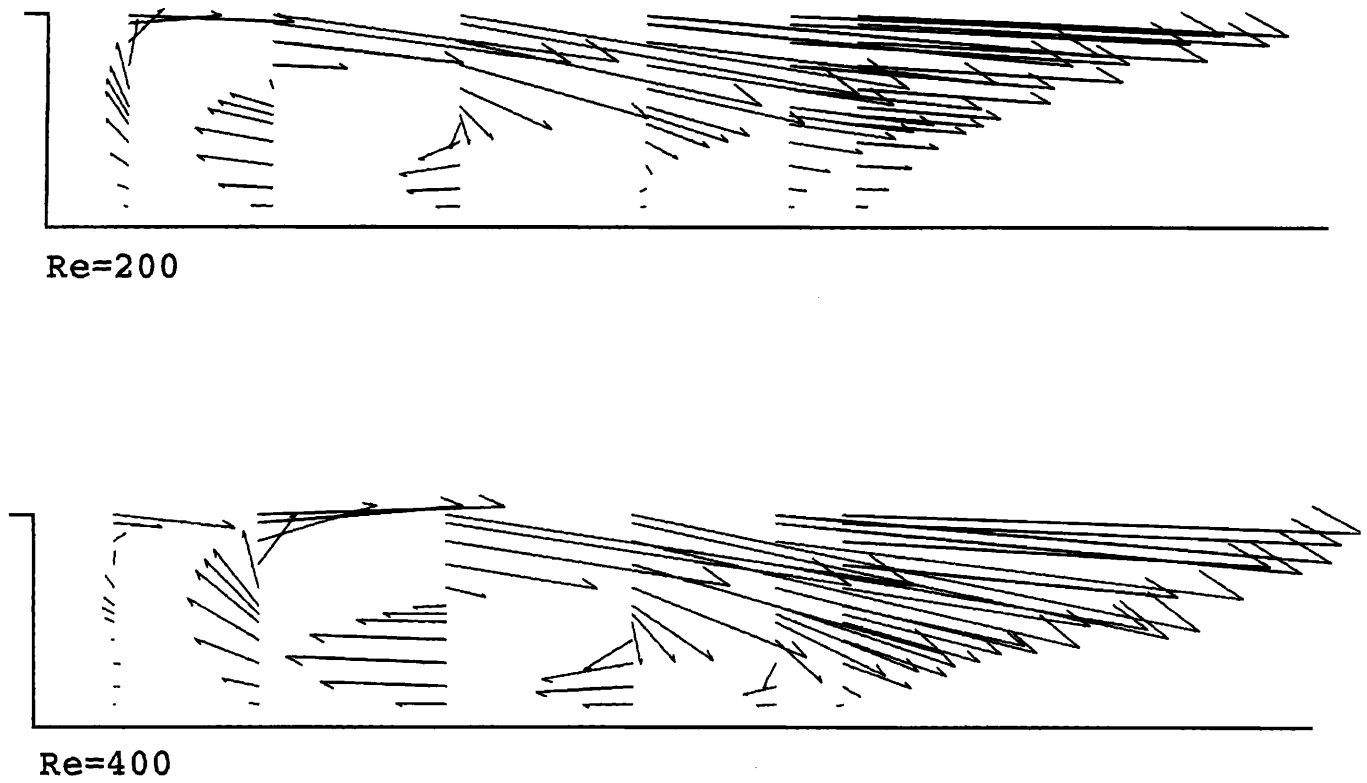


Figure 9: Vector plot focusing on the region behind the backstep for two simulations. The top simulation is from the test case $Re=200$ and the bottom simulation is from the test case $Re=400$.

